Semiempirical Investigation of Charge-Transfer Interactions in Rigid Dimethoxynaphthalene–Bridge–Pyridinium Systems

Andrew H. A. Clayton, Kenneth P. Ghiggino,* and Gerard J. Wilson†

Photophysics Laboratory, School of Chemistry, The University of Melbourne, Parkville 3054, Australia

Michael N. Paddon-Row*

School of Chemistry, The University of New South Wales, P.O. Box 1, Kensington 2033, Australia

Received: March 4, 1993; In Final Form: May 7, 1993

Semiempirical quantum chemical calculations on a series of related dimethoxynaphthalene–{polynorbornyl,-(n,σ-bonds)}–pyridine (DMN–*n*–Py) and dimethoxynaphthalene–{polynorbornyl,(n,σ-bonds)}–N-methylpyridinium (DMN–*n*–MePy$^+$) compounds have been carried out to gain insight into their electronic spectroscopy and into factors affecting photoinduced electron transfer in these novel molecular systems. The experimental electronic absorption spectra are found to be well described using the CNDO/S method. Using a simple charge–shift model and outer-sphere electron-transfer theory to take into account solvent effects, a good correlation exists between experimental charge-transfer state energies and those calculated from thermodynamic and quantum chemical treatments. The distance dependence and magnitude of the excited-state transfer integrals for photoinduced electron transfer are calculated and discussed within the framework of the McConnell model. The results of the calculations are compared with experimental data and previous studies on related DMN–*n*–dicyanovinyl donor–bridge–acceptor compounds.

Introduction

Electron-transfer (ET) processes are fundamental chemical events and are unique in that they accompany large changes in the distribution of electron density without bond formation or rupture. Their importance in biological, chemical, and physical contexts has resulted in a plethora of work from both experimental and theoretical schools.

An important advance in this field has been the rational design and synthesis of model rigid donor–bridge–acceptor (D–{bridge}–A) compounds. These systems offer the advantage that the donor and acceptor groups are held at known, well-defined distances and orientations, thereby enabling distance and orientation dependence on ET dynamics to be determined. A variety of saturated hydrocarbon bridges covalently linked to the donor and acceptor groups have been used in such studies, including the polynorbornyl (norbornylogous) bridges[1-5] cyclohexane and decalin and the steroid systems[6-10] bicyclo[2.2.2]octane,[11,12] triptycene,[13-15] and polyspirocyclobutanes.[16,17] These systems have provided invaluable rate data under a variety of conditions for comparison with existing theories of electron transfer. A number of these systems have also been studied using *ab initio* and semiempirical theoretical models.[18-29] Such studies have examined the relation between electronic structure, electronic coupling, and the rate of ET.

In the present paper, semiempirical quantum chemical calculations are carried out on a series of bichromophoric D–{bridge}–A molecules, shown in Figure 1a. These systems contain the dimethoxynaphthalene (DMN) chromophore and either the N-methylpyridinium (MePy$^+$) or the pyridine (Py) chromophore. The two chromophores are fused to the termini of a polynorbornylogous bridge of varying length. The systems are denoted DMN–*n*–MePy$^+$ or DMN–*n*–Py, where *n* denotes the number of C–C bonds in the polynorbornyl bridge directly linking the two chromophores. We have recently reported the results of photoinduced electron-transfer studies on the DMN–4–MePy$^+$, DMN–6–MePy$^+$, and DMN–6–Py systems.[5] In these studies, photoinduced ET rates of the order of 10^{10} s^{-1} were observed for DMN–4–MePy$^+$ and DMN–6–MePy$^+$, while no appreciable ET was observed for the DMN–6–Py system.

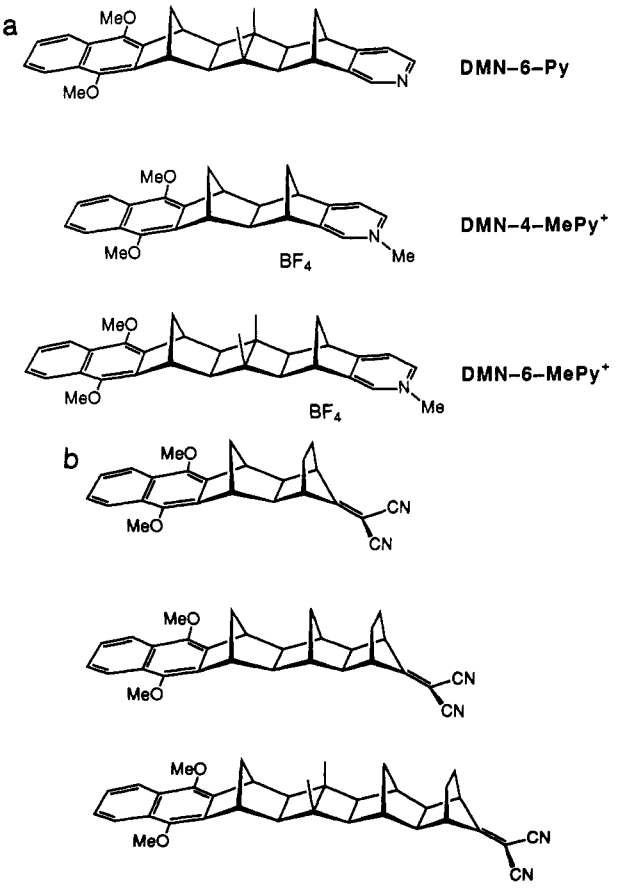

Figure 1. Rigid D–(bridge)–A systems: (a) dimethoxynaphthalene donor, pyridine or N-methylpyridinium acceptor; (b) dimethoxynaphthalene donor, dicyanovinyl acceptor.

The aim of the present work is to examine the electronic spectroscopy and the parameters affecting photoinduced electron

* Authors for correspondence.
† Present address: C.S.I.R.O. Division of Chemicals and Polymers, Private Bag 10, Clayton, Victoria 3168, Australia.

0022-3654/93/2097-7962$04.00/0

TABLE I: Chem 3D Plus MM2 Structural Parameters for DMN–*n*–MePy$^+$ and DMN–*n*–DCV Systems

system	n^a	R_e^b (Å)	R_c^c (Å)
DMN–4–MePy$^+$	4	4.8	7.6
DMN–6–MePy$^+$	6	7.2	10.1
DMN–8–MePy$^+$	8	8.8	9.9
DMN–4–DCV	4	4.6	6.7
		(4.6)	(7.0)
DMN–6–DCV	6	7.0	8.8
		(6.8)	(9.0)

[a] *n* denotes the number of C–C bonds directly linking the two chromophores. [b] Edge-to-edge separation of the two chromophores. [c] Distance separating the centroid of the donor chromophore from that of the acceptor.

transfer in these systems, including charge-transfer (CT) state energies and excited-state transfer integrals. The results are compared with the experimental electronic absorption spectra and other CNDO/S/CI calculations reported by Larsson[27-29] on the analogous polynorbornyl systems with dicyanovinyl (DCV) acceptor, denoted DMN–*n*–DCV, Figure 1b.

In section 1, we give a brief outline of the quantum chemical method used to determine the spectra and excited-state transfer integrals. In section 2, the calculated "gas-phase" spectra are used to help explain the observed electronic absorption spectra and are correlated with a simple analysis based on outer-sphere ET theory. Excited-state transfer integrals are also presented. In section 3, the results are discussed with a view to understanding the nature of electron transfer in these systems.

1. Theoretical Methods

1.1. Molecular Structures. The structural details of the molecules, obtained by molecular mechanics calculation,[30] are displayed in Table I. The data for the DMN–*n*–DCV analogues are also shown for comparison with available crystallographic data shown in parentheses.[31] R_c refers to the distance separating the centroid of the donor from that of the acceptor, and R_e is the edge-to-edge separation of the two chromophores.

1.2. Calculated Spectra ("Gas Phase"). The CNDO/S parametrization scheme has been quite popular in calculating the spectra of a variety of systems from simple aromatic chromophores to larger molecules of biological interest. Reimers and Hush[32] have used the method in conjunction with vibronic spectral fitting to infer the band origins of the ^1L_b and ^1L_a transitions of DMN, in good agreement with experimental results. Larsson *et al.* have used CNDO/S-based techniques to calculate transfer integrals in norbornylogous model bridges,[18] and they were found to be in reasonable agreement with both *ab initio* and experimental results. Larsson *et al.* have also discussed the spectra and electronic coupling in the DMN–*n*–DCV compounds.[22,27-29] We therefore expect this method to be useful in describing the spectra, CT states, and excited-state transfer integrals in the present series of compounds.

The CNDO/S method, together with configuration interaction (CI), is used to determine the spectroscopic states.[33] In this method, a Hartree–Fock SCF calculation is used to determine the CNDO/S molecular orbitals, and this is followed by a CI treatment between singly-substituted Slater determinantal basis functions. In our work, we have used about 60 configurations in the CI up to an energy expectation value of 10 eV. The Mataga–Nishimoto approximation[34] is used wherein the Coulombic repulsion integral between atoms r and s at a separation R_{rs} (in atomic units) is given by

$$\Gamma_{rs} = (R_{rs} + 2/(\Gamma_{rr} + \Gamma_{ss}))^{-1} \quad (1)$$

where Γ_{rr} and Γ_{ss} are the one-center repulsion integrals obtained from empirical data. This relationship has been shown to give good results when a small number of configurations is included in the CI.[22] The other matrix elements are approximated according to the usual CNDO/S scheme.[34]

1.3. Calculated Spectra ("Solvent"). The CNDO/S calculations neglect the role of solvent in determining the energies of CT states and are therefore "gas-phase calculations" ($\epsilon_s = 1$). As our experimental spectra have been recorded in methanol solvent, it would be desirable to have some means of correcting for this. The elongated structure of the systems being studied here makes an estimate of an effective solute cavity radius difficult and does not permit us to use an exciplex equation due to Weller.[35] Instead, we use a simple analysis based on outer-sphere ET theory.

For DMN–*n*–MePy$^+$, we write the photoinduced ET reaction as follows:

$$\text{DMN}^*\text{–}n\text{–MePy}^+ \rightarrow \text{DMN}^+\text{–}n\text{–MePy}^\bullet$$

where DMN* is the locally excited DMN donor.

We have implicitly assumed that the process is a charge-shift reaction. Provided the solvation energy of the reactants is not very different from that of the products, we may assume the free energy of the reaction to be independent of solvent and D–A separation. According to the Hush theory[36] of intervalence absorption bands, and from outer-sphere ET and solvent-dependent spectroscopic studies on related systems,[2] it can be shown that the vertical transition frequency from the ground state to the CT state may be estimated using eq 2:

$$h\nu_{ct} = \Delta G + E_{0\text{–}0} + \lambda_i + \lambda_o \quad (2)$$

where $E_{0\text{–}0}$ is the energy of the first excited DMN singlet state, ΔG is the free energy for the photoinduced ET reaction, λ_i is the intramolecular reorganization energy, and λ_o is the reorganization energy due to solvent. In the simplest model, λ_o may be expressed in terms of dielectric solvent parameters.[37]

$$\lambda_o = e^2(1/r - 1/R_c)(1/n^2 - 1/\epsilon_s) \quad (3)$$

Here r is the average ion radius (assumed to be 4.5 Å from the DMN–*n*–DCV systems[2]), R_c is the center-to-center separation (in Å), ϵ_s is the static dielectric constant, and n^2 is the square of the refractive index. For a *charge-shift* reaction, the only solvent-dependent term in eq 2 is λ_o, so to relate the CNDO/S "gas-phase" calculations to our condensed-phase measurement:

$$h\nu_{ct} = h\nu_{ct}(\text{gas phase}) + \lambda_o \quad (4)$$

For DMN–4–MePy$^+$ in a polar solvent ($\epsilon_s = 30$, $n^2 = 2$) and using eq 3, λ_o is calculated to be 0.7 eV. We have used the R_c obtained from molecular mechanics calculation (7.6 Å) while in our previous work[5] R_c was assumed to be 7 Å. This results in a difference of approximately 0.1 eV in λ_o.

For DMN–6–Py, the process is a photoinduced charge separation and the product has a large permanent dipole moment.

$$\text{DMN}^*\text{–}n\text{–Py} \rightarrow \text{DMN}^+\text{–}n\text{–Py}^-$$

Even in nonpolar solvents, the instantaneous optical solvent polarization will bring the CT state to lower energy. For polar solvents, the effect of solvation must also be considered. To estimate these effects, we use experimental redox potentials (measured in acetonitrile) and a Weller[35] expression for the reaction free energy:

$$\Delta G(R,\epsilon) = E_{0\text{–}0} + E_{ox}(\text{D}) - E_{red}(\text{A}) + \Delta G_{solv}(R,\epsilon) \quad (5)$$

The free energy is strongly dependent on the solvent polarity and magnitude of the CT state dipole moment. To calculate the transition frequency to the CT state (eq 2), we again estimate λ_o using eq 3 and assume a value for $\lambda_i = 0.6$ eV based on the DMN–*n*–DCV analogues.[2] This Weller analysis (using eqs 5 and 3) is also carried out for the DMN–*n*–MePy$^+$ systems for comparison.

1.4. Calculation of Excited-State Transfer Integrals. For electron transfer to proceed, there is a requirement that the wave functions of the donor and acceptor moieties must overlap. For bimolecular ET processes where chemically distinct moieties are

not connected to each other, they must approach closely to within the sum of their van der Waals radii before ET can take place. In D–bridge–A systems where the donor and acceptor moieties are covalently linked via a bridge, the bridge orbitals themselves can mediate this electronic interaction, by a so-called through-bond (TB) coupling mechanism.[21,23,38-40] This type of interaction results in significant electronic coupling between the donor and acceptor wave functions that extends over distances greatly exceeding the sum of their van der Waals radii. In cases where the donor and acceptor orbitals mix weakly with the bridge orbitals, the electron-transfer problem may be compactly described by a two-state system. In this situation, a transfer integral H_{rp} may be defined. H_{rp} is directly related to the rates of thermal or photoinduced electron transfer and the observed intensity of "intervalence" absorption bands. For a nonadiabatic electron transfer, assuming applicability of Fermi's golden rule, the rate may be expressed as[41,42]

$$k_{et} = (4\pi^2/h)H_{rp}^2\mathrm{FC} \tag{6}$$

where FC is a Franck–Condon factor and H_{rp}, the transfer integral, represents the electronic interaction between localized donor and acceptor states. Various expressions exist for evaluation of FC, which is related to the free energy and reorganization parameters (λ_i and λ_o) described in the previous subsection.[42] In the following, we will focus our attention on the transfer integral, H_{rp}.

H_{rp} is evaluated at the transition state which corresponds to the nuclear configuration at which the reactant and product configurations are isoenergetic. It is at this configuration that the electron can "jump" from initial to final states and satisfy the Franck–Condon principle. Physically, the transition state is realized by changes in the environment (solvent reorientation, polarization) and geometry of the D–bridge–A system. In calculational procedures, however, often *ad hoc* methods are used such as changing atomic coordinates of selected atoms or adding external electric fields to simulate solvent fluctuations. These changes are induced in the system until the "transferring" electron is delocalized 50% on both of the donor and acceptor groups. More formally, if we represent the diabatic configuration of the reactant by ψ_r (for example, D–bridge–A) and the diabatic configuration of the product by ψ_p (for example, D^+–bridge–A^-), then the electronic coupling between ψ_r and ψ_p may be described in terms of the diagonalized adiabatic states ψ_1 and ψ_2:

$$\psi_1(Q) = C_{1r}(Q)\psi_r + C_{1p}(Q)\psi_p + \dots \tag{7a}$$

$$\psi_2(Q) = C_{2r}(Q)\psi_r + C_{2p}(Q)\psi_p + \dots \tag{7b}$$

Here it is assumed that the first two terms in the expansion make the dominant contribution to the adiabatic wave functions ψ_1, ψ_2 and provide a sufficient basis set for describing the system. The coefficients in eq 7a and 7b describe the amount of mixing between the reactant ψ_r and product ψ_p configurations to produce the states ψ_1 and ψ_2, while Q is a generalized reaction coordinate. The transfer integral is assumed to be independent of Q (the Condon approximation), so Q and therefore the mixing coefficients in eqs 7a and 7b are adjustable parameters. The desired transition state is found when the energy gap between the two states ψ_1 and ψ_2 is at a minimum. Figure 2 illustrates idealized potential energy surfaces $H_{rr}(Q)$ and $H_{pp}(Q)$ for the reactants and products. The reaction coordinate, Q, describes the progress of the reaction. At the transition state $Q = Q_t$, the energies and coefficients satisfy the following relations:[43]

$$|C_{1r}/C_{1p}| = |C_{2r}/C_{2p}| = 1 \tag{8a}$$

$$|E_2 - E_1| = 2H_{rp} \tag{8b}$$

To calculate H_{rp} specifically for the DMN–*n*–$MePy^+$ systems, we require the adiabatic states ψ_1, ψ_2 formed from mixing

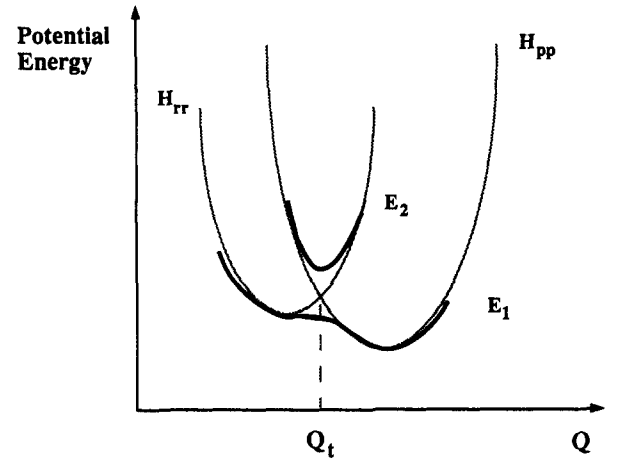

Figure 2. Reactant/product potential energy surfaces. The splitting of the adiabatic surfaces (thick line) at the activated region is indicated at Q_t.

predominantly the reactant ψ_r and product ψ_p configurations, respectively. These may be estimated using CI calculations. In our CI calculations, the reactant state (ψ_r) is a many electron wave function corresponding to a locally excited dimethoxynaphthalene donor (DMN*–*n*–$MePy^+$) and may be written

$$\psi_r = \sum C_j\psi_j \tag{9}$$

where ψ_j are singly substituted Slater determinants corresponding to single excitations between molecular orbitals essentially localized on the DMN fragment. The spectroscopy of DMN may be related to its parent chromophore naphthalene and as such can be described within the Pariser[44] model. The lowest ^1L_b state may be described as a near linear combination of HOMO − 1 → LUMO and HOMO → LUMO + 1 excitations, respectively. The next highest state ^1L_a, is described as a weaker CI between HOMO → LUMO and HOMO − 1 → LUMO + 1 excitations, respectively. The product state (DMN^+–*n*–$MePy^\bullet$) is a charge-transfer (CT) state corresponding to a single excitation from an orbital localized on the DMN donor to one on the $MePy^+$ acceptor and is approximated by a single Slater determinantal wave function:

$$\psi_p = \psi_{ct} \tag{10}$$

By substituting eqs 9 and 10 as the reactant (ψ_r) and product (ψ_p) wave functions respectively into eqs 7 and 8, the desired activated region and transfer integrals may be determined from inspection of the CI coefficients. The activated region is simulated using an external electric field while keeping the molecular geometry fixed at the ground-state geometry. This brings the product state $H_{pp}(Q)$ into crossing positions with the reactant state $H_{rr}(Q)$, as illustrated in Figure 3. The activated state is found by adjusting the electric field until two adiabatic states $\{\psi_1,\psi_2\}$ satisfying eq 8a are produced. The transfer integral is then determined using eq 8b.

1.5. Experimental Methods. Solutions of the compounds were prepared in spectroscopic grade methanol (Aldrich 99%+) and absorption spectra collected using a Hitachi Model 150-20 spectrophotometer/data processing system. Syntheses of the compounds have been reported elsewhere.[45]

2. Results

2.1. MO Energies and Calculated Spectra. The CNDO/S/CI method has been used to describe the absorption spectra of the isolated DMN donor, pyridine, and N-methylpyridinium chromophores. The calculated values are in good agreement with experimental transition energies and trends in oscillator strength. We report here our calculations for the linked DMN–*n*–$MePy^+$ and DMN–*n*–Py systems in order to obtain information about CT state energies and spectral perturbations arising from TB coupling.

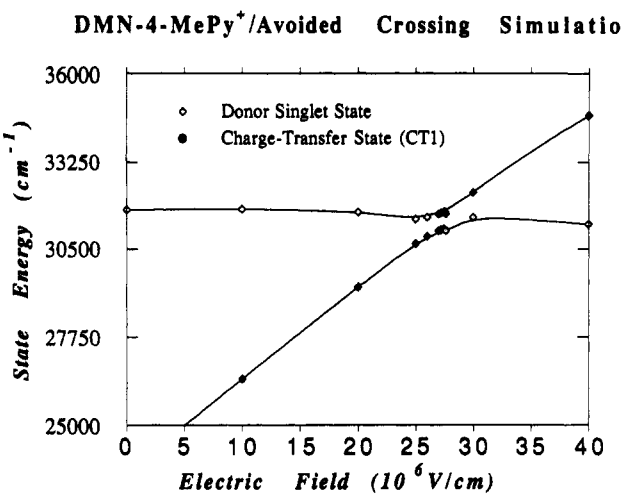

Figure 3. DMN–4–MePy$^+$ avoided crossing simulation (CNDO/S/CI, electric field method). The crossings are determined for the reactant configuration (DMN*–4–MePy$^+$) interacting with the product configuration (DMN$^+$–4–MePy*).

TABLE II: CNDO/S SCF Molecular Orbitals for DMN–6–Py

		approximate localization (DMN–bridge–Py)				approximate localization (DMN–bridge–Py)	
MO	energy (au)	DMN	Py	MO	energy (au)	DMN	Py
90	–0.016 169		Py	86[a]	–0.305 384	DMN	
89	–0.024 107	DMN	(Py)	85	–0.329 271	DMN	
88	–0.025 835	(DMN)	Py	84	–0.342 134		Py
87	–0.041 894	DMN		83	–0.367 490		Py

[a] Denotes HOMO.

TABLE III: CNDO/S SCF Molecular Orbitals for DMN–6–MePy$^+$

		approximate localization		
MO	energy (au)	DMN	*n*	MePy$^+$
94	–0.075 887	DMN		
93	–0.081 546			MePy$^+$
92	–0.093 416	DMN		
91	–0.154 493			MePy$^+$
90	–0.201 164			MePy$^+$
89[a]	–0.359 111	DMN		
88	–0.382 925	DMN		
87	–0.434 741	DMN		
86	–0.442 458	DMN		
85	–0.458 995		*n*	
84	–0.474 062	DMN–*n*–MePy$^+$		
83	–0.479 574	DMN–*n*–MePy$^+$		

[a] Denotes HOMO.

TABLE IV: CNDO/S SCF Molecular Orbitals for DMN–4–MePy$^+$

		approximate localization		
MO	energy (au)	DMN	*n*	MeP$^+$
79	–0.057 475	DMN		
78	–0.081 620			MePy$^+$
77	–0.090 697	DMN		
76	–0.107 013	DMN		
75	–0.155 154			MePy$^+$
74	–0.201 862			MePy$^+$
73[a]	–0.371 827	DMN		
72	–0.397 073	DMN		
71	–0.448 485	DMN		
70	–0.471 270	DMN–*n*–MePy$^+$		

[a] Denotes HOMO.

The CNDO/S-SCF molecular orbitals are shown in Tables II–IV. Here, we have determined the approximate localization of the molecular orbitals by inspection of the LCAO-MO coefficients. The key frontier orbitals involved in the low-energy spectroscopy and electron-transfer processes are also shown in Figure 4. The labels H and L refer to the highest occupied molecular orbital (HOMO) and lowest unoccupied molecular orbital (LUMO), respectively. CT transitions from the DMN chromophore to either Py or MePy$^+$ are indicated by the arrows.

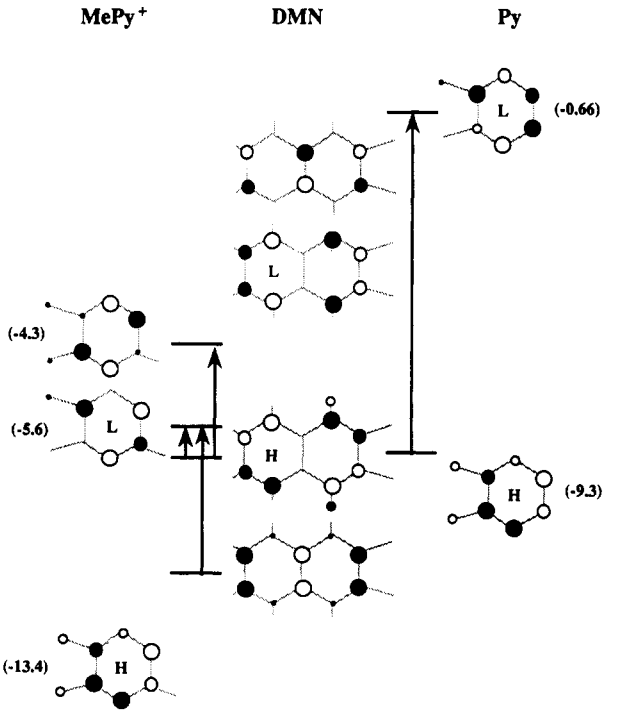

Figure 4. Frontier orbitals for isolated DMN, Py, and MePy$^+$. H and L refer to the HOMO and LUMO, respectively. The orbital energies (in eV) are shown in parentheses. CT transitions are indicated by the arrows.

The calculated line spectra for DMN–6–Py, DMN–6–MePy$^+$, and DMN–4–MePy$^+$ are displayed in Figure 5a–c.

The calculated absorption spectrum in the UV–vis region of DMN–6–Py is described solely by excitations localized on each of the DMN or Py chromophores. Thus, the spectrum is expected to be dominated by DMN transitions in the regions 310–330, 280–300, and 220–240 nm corresponding to local states with symmetries ^1L_b, ^1L_a, and ^1B_b, respectively.[2] A somewhat lower oscillator strength transition, localized on the pyridine chromophore, is also calculated in the 250–270 nm region. Some information concerning CT states can be gained from inspecting the molecular orbitals, displayed in Table II and Figure 4. As can be seen from the SCF eigenvalues, the CT excitations are at high energy and, even with a lowering of these CT states by solvent, would not be expected to appear in the absorption spectrum to any extent.

In contrast, for DMN–6–MePy$^+$, Figure 5b, several weak low-energy CT states are present, corresponding to single-electron excitations from DMN to MePy$^+$. From the SCF orbital energies, it can be seen that this is due to a lowering of the LUMO energy on the pyridinyl chromophore which is brought about by the positive charge. Four CT states are present within 2 eV of each other. This is because of the close energy separation of the HOMO and HOMO – 1 orbitals in DMN and the LUMO and LUMO + 1 orbitals in MePy$^+$, respectively. This is illustrated schematically in Figure 4. From the CT excitation energies, the energy separations of the CT states are 0.6 and 1.3 eV for CT1 – CT2 and CT1 – CT3 respectively. In addition to "pure" CT excitations, states formed from mixing (CI) between CT states and locally excited MePy$^+$ are calculated in the region. A comparison of the calculated oscillator strengths for the isolated DMN and MePy$^+$ chromophores with those of DMN–6–MePy$^+$ indicates that these perturbations to the spectrum are weak.

For DMN–4–MePy$^+$, the calculated low-energy CT states appear at similar energies to those in DMN–6–MePy$^+$. However,

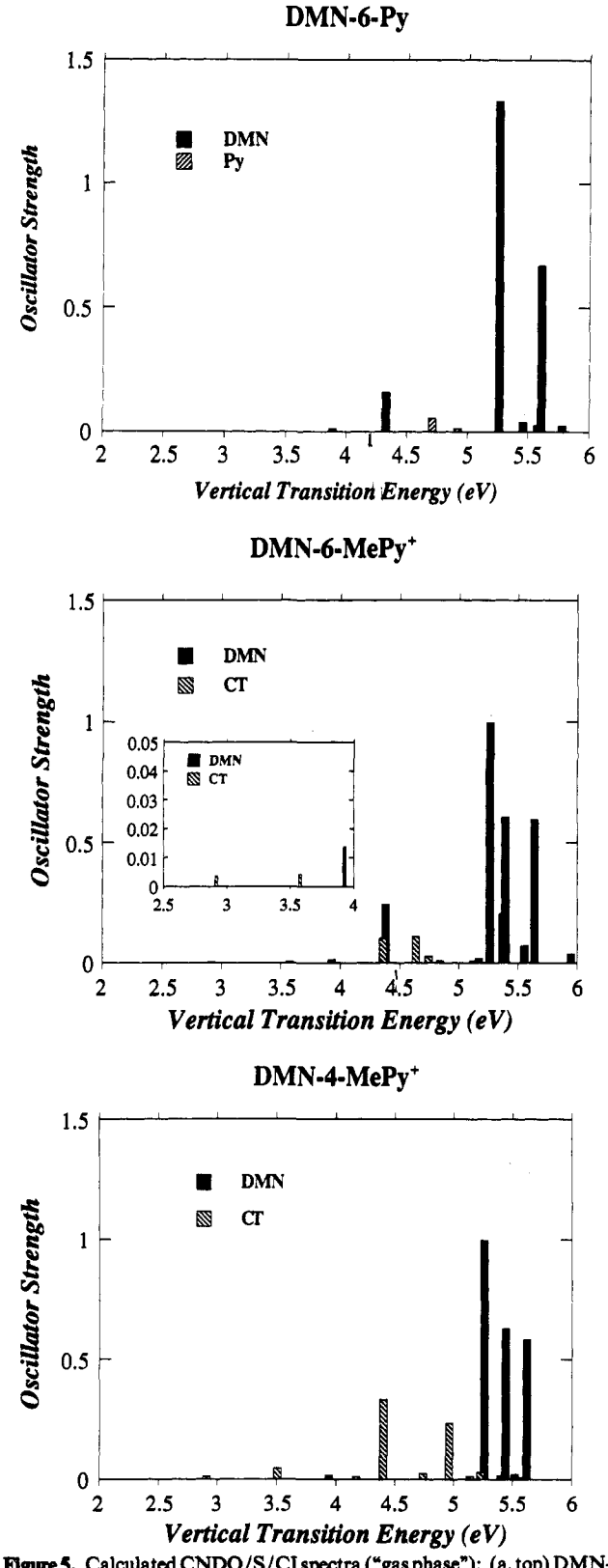

Figure 5. Calculated CNDO/S/CI spectra ("gas phase"): (a, top) DMN–6–Py, (b, middle) DMN–6–MePy+, (c, bottom) DMN–4–MePy+.

shortening of the bridge increases the calculated oscillator strength of transitions involving pure CT states and states formed from mixing of CT and local MePy+ excitations. Thus, a large increase in oscillator strength in the regions involving CT interactions is calculated.

A summary of the key CNDO/S/CI states involving a large amount of CT character is collected in Table V together with the calculated solvent "corrected" CT states, obtained using eq 4.

2.2. Electronic Absorption Spectra. The experimental absorption spectra, recorded in methanol, are depicted in Figures 6–8.

TABLE V: Comparison of Theoretical and Experimental CT Absorption Frequencies (eV)

system	CT state	CNDO/S ("gas phase")	CNDO/S ("solvent")	Weller[a]	expt
DMN–4–MePy+	CT1	2.9	3.6	3.6	3.7
	CT2	3.5	4.2	4.2	4.5
	CT3	4.2	4.9	4.8	4.9
DMN–6–MePy+	CT1	2.9	3.8	3.8	
	CT2	3.6	4.5	4.5	
	CT3	4.2	5.1	5.2	
DMN–6–Py	CTA1	–	–	5.3	
	CT2	–	–	–	
	CT3	–	–	–	

[a] Weller refers to calculated frequency using redox potentials and eqs 4 and 3.

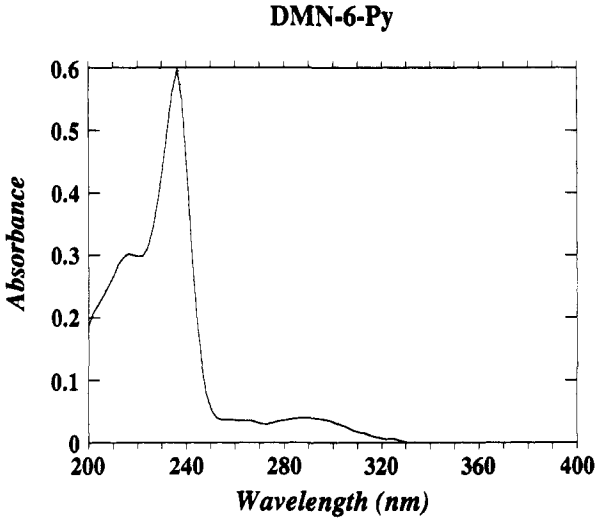

Figure 6. Electronic absorption spectrum of DMN–6–Py.

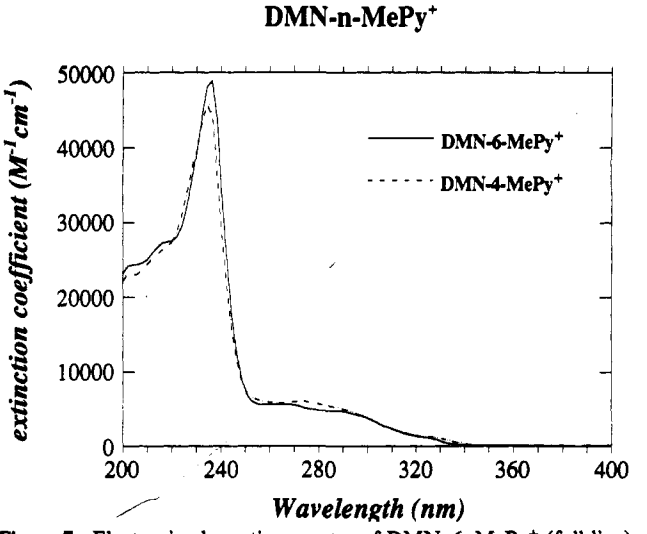

Figure 7. Electronic absorption spectra of DMN–6–MePy+ (full line) and DMN–4–MePy+ (dotted line).

The spectrum of DMN–6–Py is dominated by four broad but distinguishable peaks at 328, 290, 260, and 240 nm, respectively. In the corresponding isolated DMN chromophore, transitions at 328, 290, and 240 nm are observed corresponding to the ^1L_b and to intense vibronic progression from ^1L_a origin and ^1B_b states of DMN, respectively.[2,32] In isolated pyridine and the picolines (methylpyridines, ethanol solvent) a maximum is observed at 250–260 nm.[43] From the Weller analysis, Table VI, a CT band is anticipated at 5.3 eV (233 nm) which is just the energy of the large oscillator strength ^1B_b transition. Therefore, no conclusions regarding CT energies or interactions can be drawn from the absorption spectrum of DMN–6–Py. Most of the spectrum is essentially described by excitations localized on either chro-

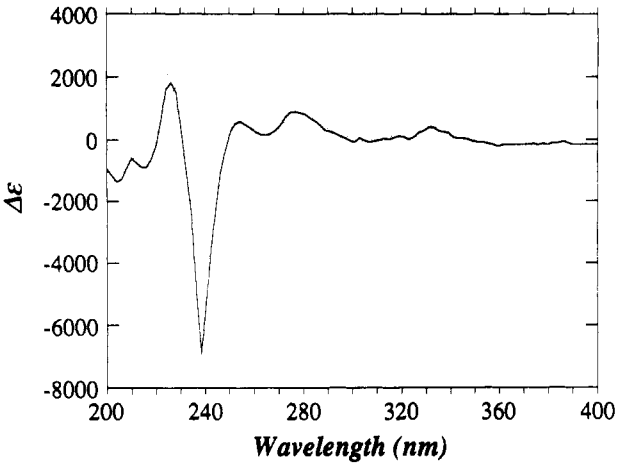

Figure 8. Difference spectrum obtained by subtracting the spectrum of DMN–6–MePy$^+$ from that of DMN–4–MePy$^+$.

TABLE VI: Summary of Excited-State Transfer Integrals (CNDO/S/CI, Electric Field Method) in cm^{-1}

system	n	$H_{CT_1 \leftarrow D^*\text{-}A}$	$H_{CT_2 \leftarrow D^*\text{-}A}$
DMN–n–MePy$^+$	4	267	193
	6	75	51
	8	16–17	16–17
DMN–n–DCV	4	533 (507)	–
	6	119 (112)	–

mophore. This is consistent with weakly interacting chromophores linked via a nonconjugated bridge.

N-Methylation of DMN–6–Py, to give DMN–6–MePy$^+$, produces a noticeable incease in intensity of the pyridinyl absorption at 260 nm. In isolated pyridine and the picolines, shifts in band energies and intensities have been observed in protic solvents and acid media. Protonation of 2- and 4-methylpyridine results in a 60% increase in oscillator strength when comparing alcoholic solvents (ethanol or water) to acidic media (sulfuric acid, 50% HCl–water).[46] Although CT absorptions are predicted, there are no appreciable perturbations in the spectrum to suggest this. Evidently the intensities of these CT transitions are very weak.

In the shorter DMN–4–MePy$^+$ analogue, Figure 7, the most notable features of the absorption spectrum are hyperchromic shifts in the wavelength regions 330–340, 270–290, and 240–260 nm. As these are not transitions found in either of the isolated chromophores, we attribute these to transitions involving CT interactions. From the difference spectrum, Figure 8, these bands are found to occur at 255, 277, and 335 nm, respectively, and are tabulated for comparison with the predicted CT states, Table V.

2.3. Excited-State Transfer Integrals. The transfer integrals for photoinduced electron transfer in the DMN–n–MePy$^+$ series of compounds have been calculated and are displayed in Table VI. We have determined these values for the ^1L_b state of DMN interacting with the lowest (CT1) and next highest (CT2) charge-transfer states, respectively. The effective transfer integrals for the third highest CT state (CT3) are not shown because the assumptions in eqs 7a and 7b are no longer valid—the two states of the system cannot be described solely by mixing of the ^1L_b state with a CT state. We have also calculated the transfer integrals for the analogous DMN–n–DCV systems as a check of our method and geometry. The corresponding values calculated by Larsson[26,29] are shown in parentheses. Here, the values have been determined for the ^1L_a state of DMN interacting with the lowest CT state. The reason for this is because at the *neutral* ground-state geometry the ^1L_b state does not interact with the CT state for reasons of symmetry. Under the overall C_s symmetry of the DMN–n–DCV systems, the locally excited ^1L_b state of DMN is symmetric with respect to the plane and the lowest CT

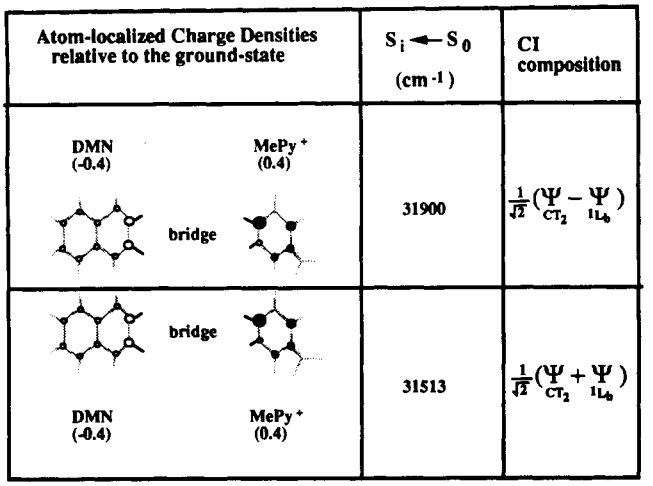

Molecule properties for a charge-separated state (CT1) in DMN-4-MePy+

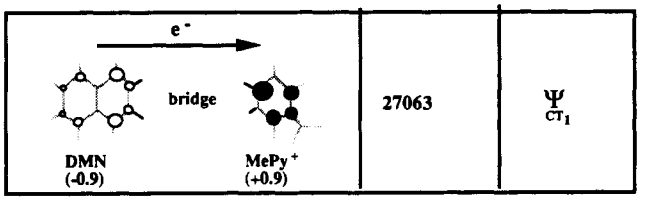

Figure 9. (top) Molecular properties of DMN–4–MePy$^+$ at the "transition" state. Note two states having equal electron density distributions are produced. The energy splitting of the two states corresponds to twice the transfer integral. (bottom) An example of the molecular properties of a CT state. Note the large change in electron density distribution.

state is antisymmetric. It is inferred from this that the fast electron transfers observed experimentally are electronically forbidden but vibronically allowed.[32] In the present DMN–n–MePy$^+$ systems, such a symmetry restriction does not apply because of the C_1 symmetry of the molecules, and thus we would expect vibronic coupling to be less important in these systems.

An example of the molecular properties calculated at the "activated region" is shown in Figure 9, for DMN–4–MePy$^+$. At this point, two states of the system are produced—the higher one an antisymmetric combination of ^1L_b and CT2 states and the lower a symmetric combination. The "charge" densities calculated at this transition state indicate that both states of the system possess an equal electron distribution on each chromophore. An example of a "pure" CT state is also shown. The large change in electron density distribution is consistent with this being a "charge-transfer" excitation.

3. Discussion

3.1. Nature of the CT States. The results of the CNDO/S/CI calculations are in good agreement with the observed absorption spectra of DMN–n–Py and DMN–n–MePy$^+$, and they qualitatively reproduce the changes in the spectra upon N-methylation of the pyridine acceptor to produce DMN–6–MePy$^+$. The calculations also reproduce observed changes in the spectra upon shortening the bridge length from DMN–6–MePy$^+$ to DMN–4–MePy$^+$. Given that these calculations are accurate to within a few tenths of an electron volt, they have described the locally excited transitions particularly well; however, states involving CT interactions are predicted at energies of the order of 1–2 eV outside the observed CT band energies as a result of solvent effects. To correct for this, we have relied on simple outer-sphere ET expressions and empirical data from "related" norbornylogous systems. Our justification for such an approach is that the rigidity of the DMN–n–Py/DMN–n–MePy$^+$ systems and their structural similarity to the well characterized DMN–n–DCV analogues mean that the parameters R_c, λ_i, and λ_o can

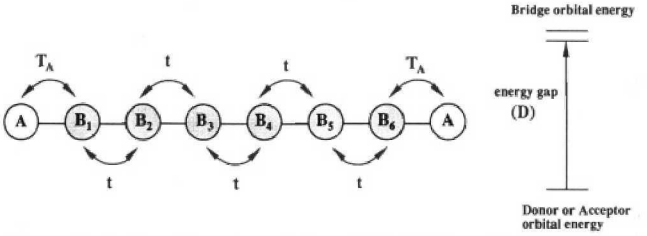

Figure 10. Schematic representation of the McConnell model.

be inferred to a reasonable degree of accuracy. The predicted positions of the CT bands are in fair agreement with those determined from difference spectroscopy, and it is pleasing that the Weller thermodynamic and quantum chemical results are in accord. The positions of the CT bands can be described in terms of the CNDO/S results. In a one-particle model, the lowest energy band (CT1) in DMN–4–MePy$^+$ involves an excitation from the HOMO (H) in DMN to the MePy + LUMO (L), the next highest CT2 band involves a DMN (H – 1) to MePy$^+$ (L) excitation, and CT3 involves a DMN (H) to MePy$^+$ (L + 1) transition. Thus, the separation of the observed first and second CT bands is attributed to the difference in energies of closely spaced *filled* orbitals in DMN while the separation of the first and third CT bands is due to the energy gap between closely spaced *vacant* MOs in MePy$^+$. From the absorption spectra, we obtain a value of 0.8 eV for the H–1 to H energy gap in DMN close to the average of the values of 0.5 and 0.9 eV inferred from a study of intermolecular CT bands involving DMN/tetracyanoethylene and in DMN–4–DCV, respectively.[2] A value of 1.2 eV is obtained for MePy$^+$ compared with the separation of intermolecular CT bands in N-methylpyridinium iodide complexes of 1 eV.[44] It should be borne in mind that in the DMN–*n*–MePy$^+$ systems the bridge between the DMN and MePy$^+$ groups plays a crucial role in mediating the CT interaction and may cause an energy rise or fall of various molecular orbitals relative to those found in the isolated chromophores. Thus, a comparison with CT data obtained from intermolecular complexes with those studied here is only intended to have qualitative, not quantitative, significance.

3.2. Transfer Integrals: Magnitude and Distance Dependence. The magnitude and distance dependence of the effective transfer integrals may be conveniently described in terms of the McConnell model,[38] which was originally developed to explain the coupling between anion states in phenyl–bridge–phenyl systems. Although this model is only approximate,[21,24] its simplicity in explaining the major physical concepts is appealing. The reader is referred to an excellent review on the McConnell model and its generalization;[21] here, we will give a brief description of the main features.

The McConnell model considers the three components, donor, bridge, and acceptor units each housing one active orbital. For a system connected by two strands of n such identical bridging units, the expression for the effective transfer integral is

$$H_{rp} = -(2T_A T_B/D)(t/D)^{n-1} \qquad (11)$$

where T_A and T_B are the matrix elements representing the coupling of the donor and acceptor to the bridge, respectively; D is the average energy gap between the orbitals of the chromophores and bridges; and t is the nearest-neighbor coupling between the adjacent bridge units. The energy gap D is defined to be positive and nearest-neighbor couplings t negative.[24] In this model, only nearest-neighbor couplings are included, so pathways involving interactions that skip over bonds are not included. These concepts are illustrated in Figure 10. Note that from eq 11 that the transfer integral follows an exponential decay with distance, viz.:

$$H_{rp} = A \exp(-\beta n) \qquad (12)$$

Here β is a decay parameter.

An additional consequence of the McConnell model is that for

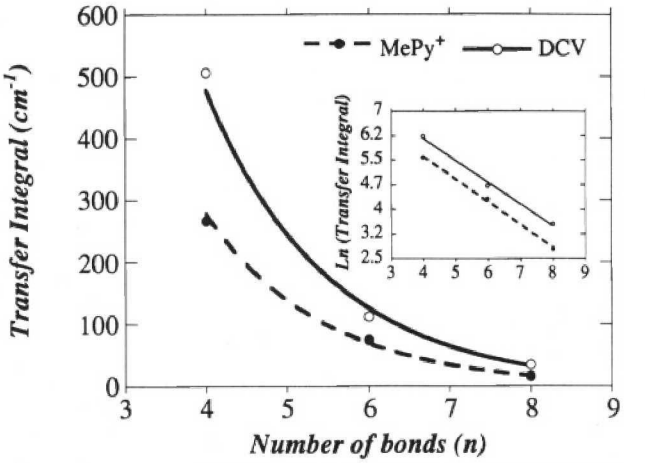

Figure 11. CNDO/S/CI excited-state transfer integrals for DMN–*n*–MePy$^+$ and DMN–*n*–DCV systems. The transfer integrals were obtained as half the splitting between the adiabatic states. Inset: Plot of ln(H_{rp}) versus the number of C–C bonds, n.

systems possessing identical bridges but different chromophores the distance dependence should be approximately the same, provided the average energy gaps (D) are similar. This implies that β values between systems with identical bridges should be transferable. In Figure 11, we have plotted the CNDO/S excited-state transfer integrals as a function of number of σ bonds for CT1 using our data for the DMN–*n*–MePy$^+$ systems, together with Larsson's[27-29] data for the DMN–*n*–DCV analogues. These systems differ only by the nature of the acceptor group. As shown in the inset of Figure 11, both fit approximately to a monoexponential distance dependence with similar decay parameters. From Larsson's data for the DMN–*n*–DCV systems,[27-29] a value of 0.67 per bond for β is obtained compared with our value of 0.69 per bond for the DMN–*n*–MePy$^+$ systems using a similar CNDO/S-based method. Although this is no verification of the McConnell model itself, it does suggest that the main component mediating the distance dependence of the transfer integral is the TB coupling through the bridge.

The actual magnitudes of the transfer integrals are difficult to obtain theoretically. However, from the McConnell model one may also derive an expression for comparing related systems with identical bridges but different chromophores. If D is approximately equal to D', then H_{rp}/H_{rp}' may be obtained by comparing the relevant chromophore bridge couplings (T, T'). An estimate of this may be obtained from the ratio of the squares of the MO coefficients at their sites of attachment to the relay. Using the CNDO/S MO's, the DCV acceptor LUMO has large MO coefficients at atoms on both strands of the polynorbornyl bridge while MePy$^+$ has a large coefficient at a single atom bonded to only one strand of the polynorbornyl bridge in mediating the electronic coupling. This effect is easily seen from the charge densities at the transition state, Figure 9. This might be a contributing factor in explaining why the CNDO/S transfer integrals for the DMN–*n*–MePy$^+$ are approximately half those of the DMN–*n*–DCV systems (cf. Table VI). We have assumed that due to the lack of symmetry in DMN–*n*–MePy$^+$ the coupling of the CT state with the ^1L_b state of DMN is similar to that with the ^1L_a state.

3.3. Implications for Photoinduced Electron Transfer. The thermodynamics of photoinduced electron transfer in DMN–*n*–MePy$^+$ may be conveniently described in terms of the free energies of the CT states. From the Weller data and absorption spectra, three CT states are thermodynamically accessible for photoinduced electron transfer at free energies of –1.5, –0.7, and –0.3 eV, respectively, independent of solvent and D–A separation. The implications for the dynamics of photoinduced electron transfer can be gleaned from comparing the positions of the CT states with the position of the first excited state of DMN. In general, activationless electron transfer will occur to a CT state

having a small vertical energy gap between itself and the locally excited DMN state. The vertical energy gap required to promote barrierless ET should be of the order of a vibrational quanta of energy, i.e., 1000–2000 cm^{-1} or less. From the experimental absorption spectrum, the vertical CT1–S_1 gap is ~800 cm^{-1} for DMN–4–$MePy^+$ and is estimated at 800 cm^{-1} in DMN–6–$MePy^+$, assuming the solvent reorganization energy in DMN–6–$MePy^+$ is 0.2 eV larger (eq 3) than that in DMN–4–$MePy^+$. Thus, both systems are expected to undergo "barrierless" electron transfer. This creates a situation where the six-bond system is slightly in the Marcus "normal region" and the four-bond system slightly in the Marcus "inverted region", which is in good agreement with our preliminary Marcus thermochemical analysis.[5] The other CT states are far removed (by 6000–10000 cm^{-1}) and are not expected to significantly contribute to the electron-transfer dynamics in polar solvents. For DMN–6–Py, we have not direct measure of the position of the CT states relative to the first excited state of DMN. However, from the Weller analysis the DMN first excited state–CT vertical energy gap is approximately 8000–10000 cm^{-1}, which presents a large barrier to the photoinduced ET reaction. This is in agreement with our observation of no electron transfer in DMN–6–Py.

From the CNDO/S calculations, only one strand of the polynorbornyl bridge is effective in mediating the ET in the DMN–*n*–$MePy^+$ systems. This may partly account for the difference in rates of photoassisted ET between these systems[5] and the DMN–4–DCV and DMN–6–DCV analogues.[2] In the latter systems, rates of the order of $1–5 \times 10^{11}$ s^{-1} were measured for the four- and six-bond compounds. Other factors such as counterion pairing with the N-methylpyridinium acceptor and specific (hydrogen-bonding) solvation effects not considered in the model may also account for the discrepancy. For the present systems, these aspects await a study of the solvent and counterion dependence.

4. Conclusions

A CNDO/S/CI quantum chemical method has been used to investigate electronic aspects of ET in a series of related dimethoxynaphthalene–{polynorbornyl}–pyridine (DMN–*n*–Py) and dimethoxynaphthalene–{polynorbornyl}–N–methylpyridinium (DMN–*n*–$MePy^+$) systems. In DMN–6–Py, no observable photoinduced ET occurs owing to all CT states being energetically well above the first excited state of DMN. Methylation of the pyridine nitrogen to produce DMN–6–$MePy^+$ results in a lowering of the LUMO energy of the acceptor chromophore, $MePy^+$, and a corresponding observed ET rate of the order of 10^{10} s^{-1}. These results agree qualitatively with a thermodynamic analysis based on experimental redox potentials. Evidence for significant electronic coupling via a through-bond interaction has been obtained by comparing the absorption spectra of DMN–6–$MePy^+$ and DMN–4–$MePy^+$. The absorption spectra of DMN–6–$MePy^+$ (and DMN–6–Py) are essentially described by excitations localized on either chromophore, while in DMN–4–$MePy^+$ there appear "new" absorption bands attributable to CT transitions from the donor chromophore to the acceptor chromophore. By using ET theory and a charge-shift model to take into account the effect of solvent on the CT state energies, the CNDO/S/CI results correlate well with the observed absorption spectra and energies of the CT states. The excited-state electronic coupling has been calculated for the DMN–*n*–$MePy^+$ series. The distance dependence (per intervening C–C bond) is found to be similar to that obtained for the analogous DMN–*n*–DCV series, indicating, as expected, that the bridge is the main component mediating the electronic coupling. The electronic coupling in the DMN–*n*–DCV systems is calculated to be twice that of the DMN–*n*–$MePy^+$ series, which partly explains the reduced photoinduced ET rates observed experimentally in the latter molecules.

In agreement with Larsson, we find the CNDO/S/CI method to be useful in describing the electronic spectra and electronic coupling in polynorbornyl-bridged D–{bridge}–A systems. This work illustrates the value of semiempirical quantum chemical methods that are currently being used to answer questions on electron-transfer interactions in large systems.

Acknowledgment. K.P.G. and M.N.P.R. thank the Australian Research Council for support. We thank Dr. J. R. Reimers and Prof. N. Hush for providing an initial version of the CNDO/S program and helpful discussions.

References and Notes

(1) Oevering, H.; Verhoeven, J. W.; Paddon-Row, M. N.; Warman, J. M. *Tetrahedron* **1989**, *45*, 4751.
(2) Oevering, H.; Paddon-Row, M. N.; Heppener, M.; Oliver, A. M.; Cotsaris, E.; Verhoeven, J. W.; Hush, N. S. *J. Am. Chem. Soc.* **1987**, *109*, 3258.
(3) Penfield, K. W.; Miller, J. R.; Paddon-Row, M. N.; Cotsaris, E.; Oliver, A. M.; Hush, N. S. *J. Am. Chem. Soc.* **1987**, *109*, 5061.
(4) Warman, J. M.; de Haas, M. P.; Paddon-Row, M. N.; Cotsaris, E.; Hush, N. S.; Verhoeven, J. W. *Nature* **1986**, *320*, 615.
(5) Clayton, A. H. A.; Ghiggino, K. P.; Wilson, G. J.; Keyte, P. J.; Paddon-Row, M. N. *Chem. Phys. Lett.* **1992**, *195*, 249–254.
(6) Calcaterra, L. T.; Closs, G. L.; Miller, J. R. *J. Am. Chem. Soc.* **1983**, *105*, 670.
(7) Closs, G. L.; Calcaterra, L. T.; Penfield, K. W.; Miller, J. R. *J. Phys. Chem.* **1986**, *90*, 3673.
(8) Closs, G. L.; Miller, J. R. *Science* **1988**, *240*, 440.
(9) Miller, J. R.; Calcaterra, L. T.; Closs, G. L. *J. Am. Chem. Soc.* **1984**, *106*, 3047.
(10) Johnson, M. D.; Miller, J. R.; Green, N. S.; Closs, G. L. *J. Phys. Chem.* **1989**, *93*, 1173.
(11) Joran, A. D.; Leland, B. A.; Geller, G. G.; Hopfield, J. J.; Dervan, P. B. *J. Am. Chem. Soc.* **1984**, *106*, 6090.
(12) Joran, A. D.; Leland, B. A.; Felker, P. M.; Zewail, A. H.; Hopfield, J. J.; Dervan, P. B. *Nature* **1987**, *327*, 508.
(13) Wasielewski, M. R.; Niemczyk, M. P.; Svec, W. A.; Pewitt, E. B. *J. Am. Chem. Soc.* **1985**, *107*, 1080.
(14) Wasielewski, M. R.; Niemczyk, M. P.; Pewitt, E. B. *J. Am. Chem. Soc.* **1985**, *107*, 5562.
(15) Wasielewski, M. R.; Niemczyk, M. P.; Johnson, D. G.; Svec, W. A.; Minsek, D. W. *Tetrahedron* **1989**, *45*, 4785.
(16) Stein, C. A.; Taube, H. *J. Am. Chem. Soc.* 1981, *103*, 693.
(17) Stein, C. A.; Lewis, N. A.; Seitz, G. *J. Am. Chem. Soc.* **1981**, *104*, 2596.
(18) Braga, M.; Broo, A.; Larsson, S. *Chem. Phys.* **1991**, *156*, 1.
(19) Braga, M.; Larsson, S. *Int. J. Quantum Chem.* **1992**, *44*, 839–851.
(20) Naleway, C. A.; Curtis, L. A.; Miller, J. R. *J. Phys. Chem.* **1991**, *95*, 8434–37.
(21) Newton, M. D. *Chem. Rev.* **1991**, *91*, 767.
(22) Larsson, S.; Broo, A.; Kallebring, B.; Volosov, A. *Int. J. Quantum Biol. Symp.* 1988, *15*, 1.
(23) Ohta, K.; Closs, G. L.; Morokuma, K.; Green, N. J. *J. Am. Chem. Soc.* **1986**, *108*, 1319.
(24) Jordan, K. D.; Paddon-Row, M. N. *Chem. Rev.* **1992**, *92*, 395–410.
(25) Ratner, M. A. *J. Phys. Chem.* **1990**, *94*, 4877.
(26) Siddarth, P.; Marcus, R. A. *J. Phys. Chem.* **1990**, *94*, 2985–2989.
(27) Larsson, S.; Volosov, A. *J. Chem. Phys.* **1986**, *85*, 2548.
(28) Larsson, S.; Volosov, A. *J. Chem. Phys.* **1986**, *86*, 5223.
(29) Larsson, S.; Volosov, A. *J. Chem. Phys.* **1987**, *87*, 6623.
(30) Chem 3D plus (MM2 energy minimization), Cambridge Scientific Computing Inc., Cambridge, MA.
(31) Craig, D. C.; Paddon-Row, M. N. *Australian J. Chem.* **1987**, *40*, 1951.
(32) Reimers, J. R.; Hush, N. S. *Chem. Phys.* **1990**, *146*, 105.
(33) Quantum Chemistry Programme Exchange no. 174.
(34) Ellis, R. L.; Kuehnlenz, G.; Jaffe, H. H. *Theor. Chim. Acta* **1972**, *26*, 131.
(35) Weller, A. *Z. Physik. Chem. NF* **1982**, *133*, 93–98.
(36) Hush, N. S. *Prog. Inorg. Chem.* **1967**, *30*, 1.
(37) Hush, N. S. *Trans. Faraday Soc.* **1961**, *57*, 557.
(38) McConnell, H. M. *J. Chem. Phys.* **1961**, *35*, 508.
(39) Hoffmann, R.; Imamura, A.; Hehre, W. J. *J. Am. Chem. Soc.* **1968**, *90*, 1499.
(40) (a) Hoffmann, R. *Acc. Chem. Res.* **1971**, *94*, 71. (b) Paddon-Row, M. N. *Acc. Chem. Res.* **1982**, *15*, 245.
(41) Kestner, N. R.; Jortner, J.; Logan, J. *J. Phys. Chem.* **1974**, *78*, 2148.
(42) Marcus, R. A.; Sutin, N. *Biochim. Biophys. Acta* **1985**, *811*, 265.
(43) Bertrand, P. *Structure and Bonding* **1991**, *75*, 1–47.
(44) Pariser, R. *J. Chem. Phys.* **1956**, *24*, 250.
(45) Jaffe, H. H.; Orchin, M. *Theory and Applications of Ultraviolet Spectroscopy*; John Wiley and Sons: New York, London, 1962; pp 361–367.
(46) Verhoeven, J. W.; Dirkx, I. P.; de Boer, T. J. *Tetrahedron* **1969**, *25*, 3395.
(47) Golka, A.; Keyte, P. J.; Paddon-Row, M. N. *Tetrahedron* **1992**, *48*, 7663.